

Corrections

CELL BIOLOGY

Correction for “A distinct pool of phosphatidylinositol 4,5-bisphosphate in caveolae revealed by a nanoscale labeling technique,” by Akikazu Fujita, Jinglei Cheng, Kumi Tauchi-Sato, Tadaomi Takenawa, and Toyoshi Fujimoto, which appeared in issue 23, June 9, 2009, of *Proc Natl Acad Sci USA* (106:9256–9261; first published May 22, 2009; 10.1073/pnas.0900216106).

The authors note that on page 9257, Figure 1 appeared incorrectly. This error does not affect the conclusions of the article. The corrected figure and its legend appear below.

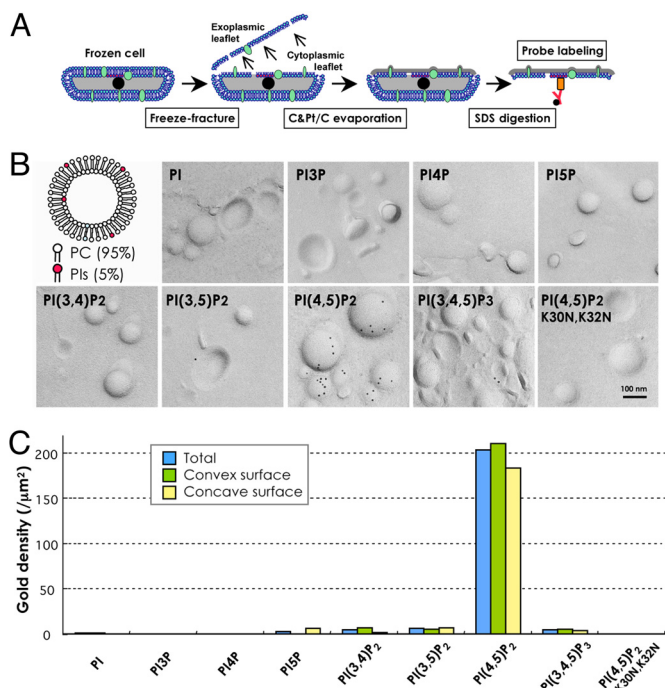


Fig. 1. Labeling of the liposome. (A) Outline of the method. Cells were rapidly frozen, freeze-fractured, and evaporated with carbon (C) and platinum/carbon (Pt/C) in vacuum. The replica of the split membrane was digested with SDS to remove noncast molecules and labeled by GST-PH. Both the cytoplasmic and exoplasmic halves of the membrane were examined. (B) Labeling of small unilamellar liposome replicas. Freeze-fracture replicas of liposomes containing 95 mol % of phosphatidylcholine (PC) and 5 mol % of phosphatidylinositol or a phosphoinositide were labeled. Only liposomes containing PI(4,5)P₂ were labeled intensely by GST-PH. A PH mutant, GST-PH(K30N, K32N), which does not bind PI(4,5)P₂, showed little labeling in the PI(4,5)P₂-containing liposome. (C) Quantification of the GST-PH labeling in the liposomes. The number of gold particles per 1 μm² of the liposome surface is shown (blue). The labeling on the convex (green) and concave (yellow) surfaces showed equivalent results.

www.pnas.org/cgi/doi/10.1073/pnas.0906215106

CELL BIOLOGY

Correction for “Reprogramming of murine and human somatic cells using a single polycistronic vector,” by Bryce W. Carey, Styliani Markoulaki, Jacob Hanna, Kris Saha, Qing Gao, Maisam Mitalipova, and Rudolf Jaenisch, which appeared in issue 1, January 6, 2009, of *Proc Natl Acad Sci USA* (106:157–162; first published December 24, 2008; 10.1073/pnas.0811426106).

“The authors inadvertently neglected to state that, at the time of publication, RJ was an advisor to Fate Therapeutics. We regret this error.”

www.pnas.org/cgi/doi/10.1073/pnas.0906359106

CHEMISTRY

Correction for “Development of aliphatic biodegradable photoluminescent polymers,” by Jian Yang, Yi Zhang, Santosh Gautam, Li Liu, Jagannath Dey, Wei Chen, Ralph P. Mason, Carlos A. Serrano, Kevin A. Schug, and Liping Tang, which appeared in issue 25, June 23, 2009, of *Proc Natl Acad Sci USA* (106:10086–10091; first published June 8, 2009; 10.1073/pnas.0900004106).

The authors note that due to a printer’s error, Fig. 3B appeared incorrectly. The corrected figure and its legend appear below.

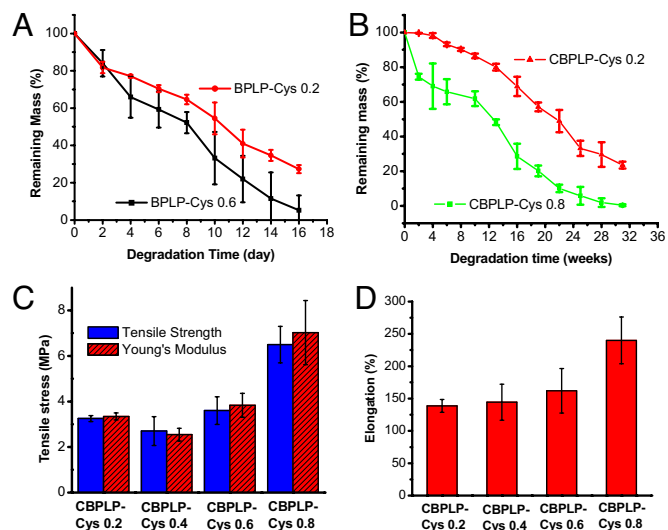


Fig. 3. Studies of polymer degradation and mechanical properties. (A) In vitro degradation of BPLP-Cys in PBS (pH = 7.4) at 37 °C (n = 5). (B) In vitro degradation of CBPLP-Cys in PBS (pH = 7.4) at 37 °C (n = 5). (C) Tensile strength and initial Young’s modulus of CBPLP-Cys synthesized with various molar concentration of L-cysteine (n = 5). (D) Elongation of CBPLP-Cys synthesized with various molar concentration of L-cysteine (n = 5).

www.pnas.org/cgi/doi/10.1073/pnas.0906520106

Development of aliphatic biodegradable photoluminescent polymers

Jian Yang^{a,b,1}, Yi Zhang^{a,b}, Santosh Gautam^{a,b}, Li Liu^c, Jagannath Dey^{a,b}, Wei Chen^d, Ralph P. Mason^{b,c}, Carlos A. Serrano^e, Kevin A. Schug^e, and Liping Tang^{a,b}

Departments of ^aBioengineering, ^dPhysics, and ^eChemistry and Biochemistry, University of Texas, Arlington, TX 76019; ^bJoint Biomedical Engineering Program, University of Texas at Arlington and University of Texas Southwestern Medical Center, Dallas, TX 75390; and ^cDepartment of Radiology, Advanced Radiological Sciences, University of Texas Southwestern Medical Center, Dallas, TX 75390

Edited by Robert Langer, Massachusetts Institute of Technology, Cambridge, MA, and approved April 30, 2009 (received for review January 8, 2009)

None of the current biodegradable polymers can function as both implant materials and fluorescent imaging probes. The objective of this study was to develop aliphatic biodegradable photoluminescent polymers (BPLPs) and their associated cross-linked variants (CBPLPs) for biomedical applications. BPLPs are degradable oligomers synthesized from biocompatible monomers including citric acid, aliphatic diols, and various amino acids via a convenient and cost-effective polycondensation reaction. BPLPs can be further cross-linked into elastomeric cross-linked polymers, CBPLPs. We have shown representatively that BPLP-cysteine (BPLP-Cys) and BPLP-serine (BPLP-Ser) offer advantages over the traditional fluorescent organic dyes and quantum dots because of their preliminarily demonstrated cytocompatibility *in vitro*, minimal chronic inflammatory responses *in vivo*, controlled degradability and high quantum yields (up to 62.33%), tunable fluorescence emission (up to 725 nm), and photostability. The tensile strength of CBPLP-Cys film ranged from 3.25 ± 0.13 MPa to 6.5 ± 0.8 MPa and the initial Modulus was in a range of 3.34 ± 0.15 MPa to 7.02 ± 1.40 MPa. Elastic CBPLP-Cys could be elongated up to 240 \pm 36%. The compressive modulus of BPLP-Cys (0.6) (1:1:0.6 OD:CA:Cys) porous scaffold was 39.60 ± 5.90 KPa confirming the soft nature of the scaffolds. BPLPs also possess great processability for micro/nanofabrication. We demonstrate the feasibility of using BPLP-Ser nanoparticles ("biodegradable quantum dots") for *in vitro* cellular labeling and noninvasive *in vivo* imaging of tissue engineering scaffolds. The development of BPLPs and CBPLPs represents a new direction in developing fluorescent biomaterials and could impact tissue engineering, drug delivery, bioimaging.

bioimaging | elastomers | photoluminescence | tissue engineering

A unique biomaterial may create new fields of study and opportunities to tackle unmet scientific problems. The discovery of fluorescent quantum dots is a good example (1–4). The unique photoluminescent properties of fluorescent quantum dots bring tremendous opportunities for cancer therapy and diagnosis through biological labeling and imaging. Similarly, fluorescent protein has become one of the most important tools in bioscience, because it can reveal processes previously invisible. Fluorescent biomaterials have been an intense research focus in biomedical and biological fields with wide applications in cellular imaging, biosensing, immunology, drug delivery and tissue engineering (5–10). Current fluorescent biomaterials include fluorescent organic dyes, fluorescent proteins, lanthanide chelates, and quantum dots. Most of the organic dyes such as fluoresceins, rhodamines, and cyanine dyes are not used *in vivo* because they exhibit poor photostability and substantial cytotoxicity (11, 12). Fluorescent proteins often suffer from photobleaching (13, 14) and low quantum yield (15). Furthermore, the aggregation of fluorescent proteins inside cells may cause cellular toxicity (16). Although various surface modifications have been attempted to reduce their toxicity (9, 12, 17, 18), the accumulation of toxic ions released from quantum dots remains a significant concern, especially for long-term use *in vivo*.

Synthetic fluorescent polymers have been developed for various nonbiological applications, such as light emitting diodes (19). These polymers are not degradable and usually contain conjugated phenyl units raising concerns of potential carcinogenesis or toxicity when used for *in vivo* biomedical applications. Hitherto, biodegradable fluorescent polymers have required conjugation or encapsulation of the organic dyes or quantum dots on or in the degradable polymers to be visualized (11, 20–23). However, these approaches do not address the previously mentioned drawbacks of the organic dyes and quantum dots. Thus, there is an urgent need for the development of biodegradable and biocompatible photoluminescent materials.

In this study, we report the development of aliphatic biodegradable synthetic polymers, which show intriguing photoluminescence phenomena. A series of biodegradable photoluminescent polymers (BPLPs) are described. BPLPs are low-molecular-weight aliphatic oligomers that include both water-soluble and water-insoluble oligomers. They can be further processed to form elastomeric cross-linked BPLPs (CBPLPs), which not only possess desirable mechanical properties, but also retain strong, tunable fluorescence emission ranging from blue to red. Tunability is afforded by the incorporation of different amino acid residues during polymer synthesis. CBPLPs have potential for use as implant or device materials and, in addition, as *in vivo* bioimaging probes. We have examined the *in vitro* cellular uptake of fluorescent BPLP nanoparticles and conducted *in vivo* fluorescence bioimaging of CBPLP scaffolds to demonstrate their potential use in cellular fluorescence labeling, drug delivery and tissue engineering. We further present evidence related to their *in vitro* degradation and proffer a mechanism through which the photoluminescence of these promising materials is achieved.

Results and Discussions

Synthesis and Characterization of the BPLP Families. The syntheses of BPLPs and CBPLPs are straightforward and similar to that for the previously developed biodegradable elastomers, poly(octamethylene citrates) (POC) (24, 25). For the synthesis of POC, citric acid (CA) was reacted with 1,8-octanediol (OD) via a condensation reaction to form an oligomer referred to as pre-POC. Pre-POC was then postpolymerized through further condensation to form an elastomeric cross-linked polymer network. Similarly, any of the twenty (enantiomerically pure (*L*-)) amino acids were added into the reaction of citric acid and 1,8-octanediol to prepare a family of oligomeric BPLPs such as

Author contributions: J.Y. designed research; J.Y., Y.Z., S.G., L.L., J.D., C.A.S., and K.A.S. performed research; J.Y., Y.Z., S.G., L.L., J.D., W.C., R.P.M., K.A.S., and L.T. analyzed data; and J.Y. wrote the paper.

The authors declare no conflict of interest.

This article is a PNAS Direct Submission.

¹To whom correspondence should be addressed. E-mail: jianyang@uta.edu.

This article contains supporting information online at www.pnas.org/cgi/content/full/090004106/DCSupplemental.

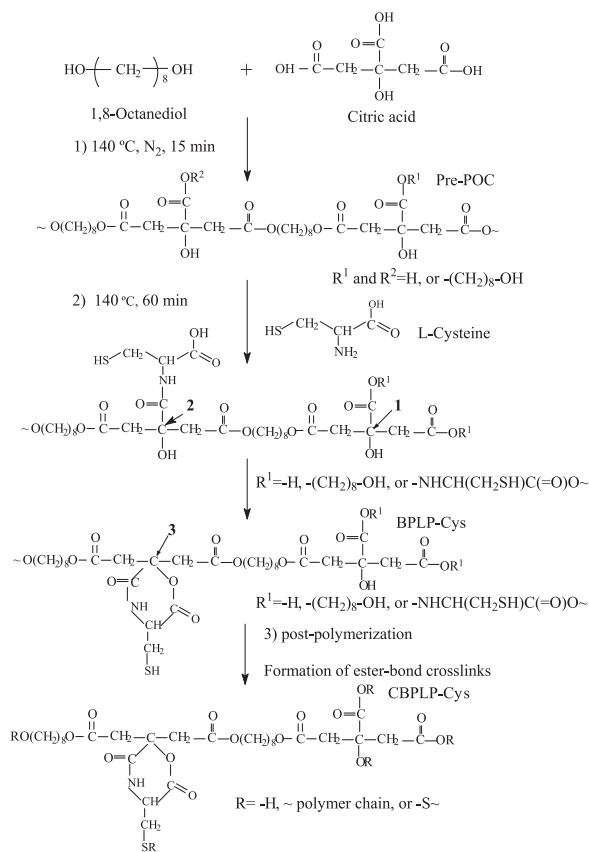


Fig. 1. Synthesis schematics for BPLP-Cys.

BPLP-cysteine (BPLP-Cys or POC-Cys) and BPLP-serine (BPLP-Ser or POC-Ser). BPLPs could be further postpolymerized to form CBPLPs. BPLPs were soluble in organic solvents such as 1,4-dioxane, ethanol, acetone, and tetrahydrofuran when hydrophobic diols such as 1,8-octanediol were used. Water soluble BPLPs could be synthesized using hydrophilic diols such as poly(ethylene glycol) (e.g., PEG 200 and PEG 400).

Polymer characterizations were conducted for BPLP-Cys as a representative BPLP, except where otherwise specified. The proposed polymer structures are shown in Fig. 1. The FTIR spectra (Fig. S1A) confirmed the presence of $-\text{SH}$ at $2,575\text{ cm}^{-1}$, $-\text{C}(=\text{O})\text{NH}-$ at $1,527\text{ cm}^{-1}$, $-\text{C}=\text{O}$ at $1,731\text{ cm}^{-1}$, $-\text{CH}_2-$ at $2,931\text{ cm}^{-1}$, and $-\text{OH}$ at $3,467\text{ cm}^{-1}$. In the $^1\text{H-NMR}$ spectra of BPLP-Cys (Fig. S1B), the presence of the peaks at 1.02 ppm ($-\text{CH}_2\text{SH}$ from L-cysteine), 1.23 ppm and 1.50 ppm ($-\text{CH}_2-$ from 1,8-octanediol), and the multiple peaks at 2.75 ppm ($-\text{CH}_2-$ from citric acid) confirmed the incorporation of L-cysteine into pre-POC. In the $^{13}\text{C-NMR}$ spectra of BPLP-Cys (Fig. S1C), the peaks ≈ 170 ppm were assigned to carbonyl ($\text{C}=\text{O}$) groups from citric acid and L-cysteine. The peaks ≈ 63.8 ppm and 28.5 ppm were assigned respectively to $-\text{O}-\text{CH}_2\text{CH}_2-$ and $-\text{O}-\text{CH}_2\text{CH}_2-$ from 1,8-octanediol. The $-\text{C}(=\text{O})-\text{CH}_2-$ carbon from citric acid was assigned to the peak at 61.2 ppm. The $-\text{HN}-\text{CH}-$ carbon from L-cysteine was assigned to the peak at 54.5 ppm. There were 4 peaks assigned to the central carbon atoms of citrate units in various chemical environments. Peaks at 72.9 and 73.4 were assigned to C1 when R^1 is $-(\text{CH}_2)_8-\text{OH}$ and $-\text{H}$ respectively. Peaks at 72.1 and 72.4 ppm were assigned to C2 and C3 respectively. However, the $^{13}\text{C-NMR}$ of pre-POC only showed 2 peaks of central C of citrate units at 72.9 and 73.4 ppm. The $^{13}\text{C-NMR}$ results suggest the presence of a 6-mem-

bered ring formed on BPLP-Cys as depicted in Fig. 1. A 6-membered ring formed between L-cysteine and hydroxyl groups on the central C of the citrate unit is proposed to be responsible for the fluorescence as discussed below. The average molecular mass of BPLP-Cys-0.2 (formed by reaction of 1:1:0.2 OD:CA:Cys) measured by MALDI-MS was 1,334 Da (Fig. S2). The above polymer characterization confirmed that L-cysteine was incorporated into the BPLP-Cys. The overall BPLP synthesis is believed to have resulted in a blend of oligomers of POC (pre-POC) and BPLP-Cys as shown in Fig. 1 due to the low percentage of L-cysteine in the polymers.

Photoluminescence Properties of BPLPs and CBPLPs. The various forms of BPLPs, including BPLP solution (Fig. 2A), CBPLP films (Fig. 2B), CBPLP scaffolds (Fig. 2C), and BPLP nanoparticles (Fig. 2D), all emit strong fluorescence. The fluorescence intensity of BPLP-Cys can be tuned by varying the molar concentration of L-cysteine in the polymers (Fig. 2A). Fig. 2E shows that BPLP-serine (BPLP-Ser) emits different fluorescent colors from blue to red depending on the excitation wavelength. To further explore this class of material, we have synthesized a family of BPLPs using each of the 20 natural amino acids. The BPLPs were found to exhibit fluorescence colors ranging from blue to red (up to 725 nm) (Table 1) depending on the choice of amino acid.

The fluorescence intensity of BPLP-Cys decreased only slightly ($<2\%$) after continuous UV excitation for 3 h indicating excellent photostability as compared with the organic fluorescent dye rhodamine-B (Fig. 2F). The quantum yields of the BPLP-Cys (62.3%) and BPLP-Ser (26.0%) (Fig. 2G and Table 1) were much higher than those reported for fluorescent proteins such as green fluorescent protein (GFP) (7.3%) and its blue variants (7.9%) (15). The emission range and quantum yields of all BPLPs are listed in Table 1. The fluorescence intensity of BPLP-Cys-0.2 increased with increasing degradation in NaOH solution (Fig. S3A). It should be noted that the fluorescence measurements for polymers under degradation were based on the same concentration of BPLP-Cys in 1,4-dioxane at various degrees of degradation. MALDI-MS analysis indicated that the molecular mass of the insoluble polymer did not significantly change during degradation in NaOH solution (Fig. S3B). We suspect that the polymers containing fluorescent ring-structures may degrade more slowly than the polymers without the ring-structures (pre-POC) because of the relatively higher stability of the amide bonds in the ring-structures. Considering that the molecular mass of pre-POC ($M_n = 1,088$ Da) (25) is close to that of M_w of the resulting BPLP-Cys, which may contain pre-POC, the degradation may result in an erosion on the pre-POC first, leaving behind the low percentage of BPLP-Cys without significant molecular mass changes. Therefore, the polymer degradation is proposed to have resulted in an increasing concentration of the polymer chains with the fluorescent ring-structures.

Exploration of the Fluorescence Mechanism. The intriguing photoluminescent properties of the BPLP families encouraged us to explore potential mechanisms for the fluorescence. As shown in Fig. 2H, monomers of citric acid, 1,8-octanediol, and L-cysteine emitted only very weak autofluorescence. The POCs synthesized from citric acid and 1,8-octanediol also emitted negligible photoluminescence. However, when L-cysteine was incorporated into POC (BPLP-Cys), a strong fluorescence signal was observed. We attempted to directly synthesize polymers from citric acid and L-cysteine or 1,8-octanediol and L-cysteine, but failed because the melting point of L-cysteine ($220\text{ }^\circ\text{C}$) is much higher than the decomposition temperature of citric acid ($175\text{ }^\circ\text{C}$). However, when 1,8-octanediol was reacted first with citric acid, the formed pre-POC could then dissolve L-cysteine at $160\text{ }^\circ\text{C}$ to form BPLP-Cys. It is reasonable to suggest that during this synthesis the L-cysteine might be either incorporated in the

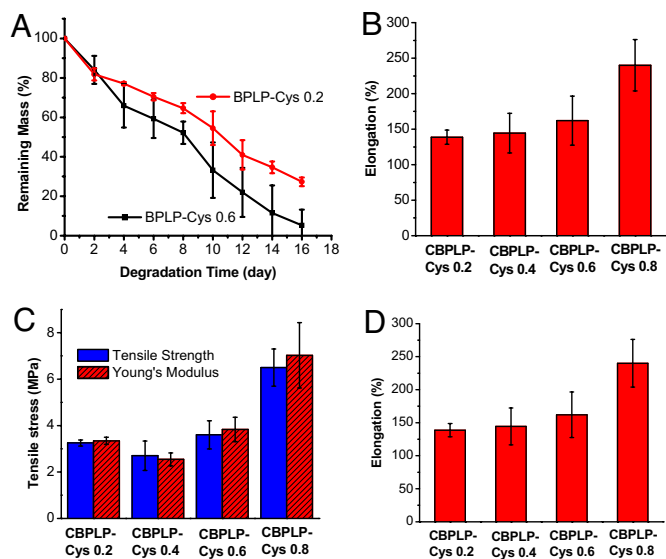


Fig. 3. Studies of polymer degradation and mechanical properties. (A) In vitro degradation of BPLP-Cys in PBS (pH = 7.4) at 37 °C ($n = 5$). (B) In vitro degradation of CBPLP-Cys in PBS (pH = 7.4) at 37 °C ($n = 5$). (C) Tensile strength and initial Young's modulus of CBPLP-Cys synthesized with various molar concentration of L-cysteine ($n = 5$). (D) Elongation of CBPLP-Cys synthesized with various molar concentration of L-cysteine ($n = 5$).

6.5 ± 0.8 MPa and the initial Modulus was in a range of 3.34 ± 0.15 MPa to 7.02 ± 1.40 MPa, which were stronger than those of POC elastomers (25). CBPLP-Cys could be elongated up to $240 \pm 36\%$, which is comparable with reports of such values for arteries and veins (25). The compressive modulus of BPLP-Cys (0.6) (1:1:0.6 OD:CA:Cys) scaffold was 39.60 ± 5.90 KPa confirming the soft nature of the scaffolds, similar to that reported for soft elastomers including poly(diols citrates) (POC), poly(glycerol sebacate) and xylitol-based polymers (25, 27–30).

Cytotoxicity Evaluation and Bioimaging Study in Vitro and in Vivo.

Cyto-compatibility of BPLPs and CBPLPs and their potential applications for cellular bioimaging, drug delivery, and tissue engineering were evaluated (Fig. 4). CBPLP-Cys films were found to support 3T3 mouse fibroblast adhesion and proliferation. Viable cell numbers on CBPLPs were significantly higher than those on controls POC film and poly(D,L-lactide-co-glycolide) (PLGA 75/25) film at day 7 ($P < 0.05$) (Fig. 4A). Importantly, cytotoxicity evaluation for degradation products suggested that the degradation of BPLPs and CBPLPs generated similar cytotoxicity to the controls POC and PLGA75/25 ($P > 0.05$) (Fig. 4B). When implanted in vivo, the CBPLP-Ser scaffolds did not trigger noticeable edema and tissue necrosis on the tested animals. Samples that were implanted for 5 months produced a thin fibrous capsule, characteristic of a weak chronic inflammatory response (Fig. S5), which was expected and consistent with the introduction of foreign materials into the body. Intake of BPLP-Ser nanoparticles by cells generated cells labeled with various fluorescence colors (Fig. 4 C–E). After s.c. implantation in nude mice, BPLP-Ser nanoparticles and CBPLP-Ser scaffolds (Fig. 4G) were readily detected in vivo, using a noninvasive imaging system (Fig. 4 F and H). Extensive investigation of relevant in vivo degradation mechanisms for these materials is currently underway.

The potential future applications of the unique BPLP families are worthy of further note. BPLPs can be used as fluorescence probes offering advantages over the traditional organic dyes and semiconductor quantum dots because of their tunable fluorescence emission, high quantum yield, degradability, photostabil-

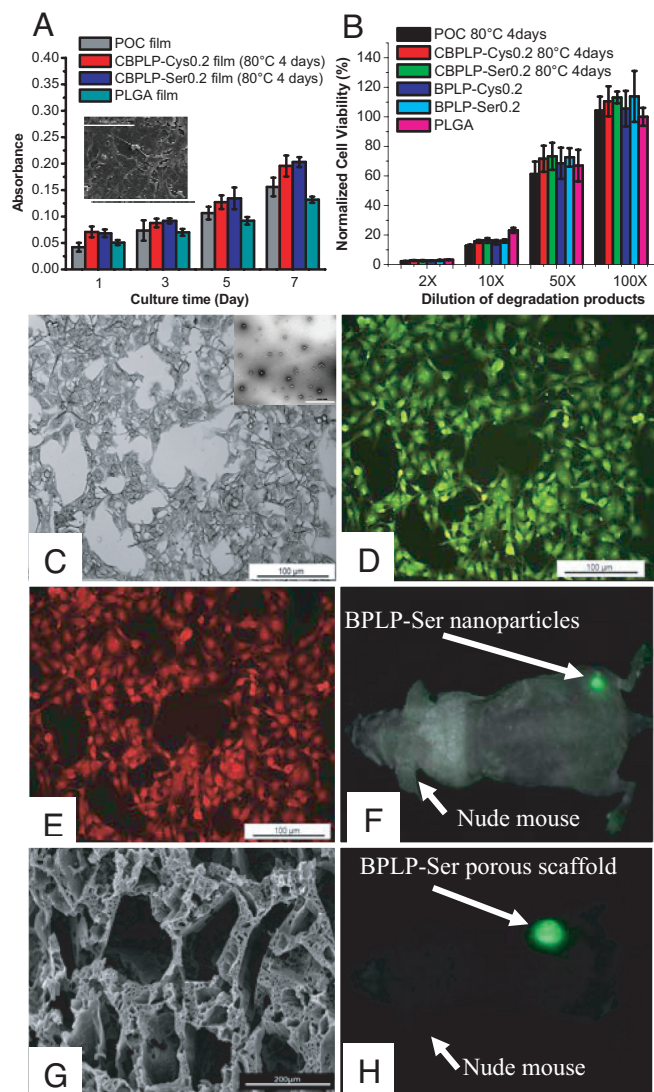


Fig. 4. Cell culture studies and fluorescence imaging studies in vitro and in vivo. (A) Cell viability and proliferation assay (MTT assay) for 3T3 fibroblasts cultured on BPLP-Cys film. POC and PLGA were used as controls. (A Inset) A SEM picture of 3T3 fibroblasts cultured on CBPLP-Cys-0.2 film. (B) Cytotoxicity evaluation of degradation products of BPLPs (-Cys and -Ser) and CBPLPs (-Cys and -Ser) at 2 \times , 10 \times , 50 \times and 100 \times dilutions. POC and PLGA75/25 were used as controls. All data were normalized to the mean absorbance of PLGA (100 \times dilution). (C) BPLP-Ser nanoparticle-uptaken 3T3 fibroblasts observed under the light microscope (20 \times). (C Inset) A TEM picture of BPLP-Ser nanoparticles (80 nm). (D and E) BPLP-Ser nanoparticle-uptaken 3T3 fibroblasts observed under fluorescent microscope with FITC filter (20 \times) and with Texas Red filter (20 \times). (F) Fluorescence image of BPLP-Ser nanoparticles injected s.c. in a nude mouse. (G) SEM image of the cross section of a porous BPLP-Ser scaffold. (H) Fluorescence image of BPLP-Ser porous scaffold implanted s.c. in a nude mouse. (Scale bars: C–E, 100 μ m; C Inset, 1,000 nm; G, 200 μ m.)

ity, and cell compatibility. We have shown that BPLP nanoparticles (“biodegradable quantum dots”) can be used to label cells. Thus, it may be possible to develop a biodegradable fluorescent drug delivery system using BPLPs avoiding the long-term toxicity associated with current labels. The low-molecular mass BPLPs can be made to be water-insoluble or -soluble maximizing their potential applications in biological labeling and imaging. The water soluble low-molecular-weight BPLPs may potentially be used for single molecule labeling such as protein and DNA labeling in proteomics and genomics research, where quantum

dots may not be ideal because of their size (7, 8). The BPLP family may also be suitable for use in fluorescence resonance energy transfer (FRET) (5), 2-photon excited fluorescence microscopy (6), multimodal compositions (combined with magnetic or radionuclear agents) (31), and biosensors (32). BPLP polymers provide real promise for noninvasive real-time monitoring of the scaffold degradation and tissue infiltration/formation *in vivo*, which has been a challenge in the evolving field of tissue engineering (33–35). Our results have demonstrated that the fluorescent BPLP nanoparticles and CBPLP scaffolds could be imaged *in vivo* with negligible interference from tissue autofluorescence. We believe that the *in vivo* scaffold bioimaging will open new avenues for soft tissue engineering studies and may provide an opportunity for doctors to track clinical outcomes without an open surgery.

Summary. We report the discovery of a family of aliphatic biodegradable photoluminescent polymers (BPLPs and CBPLPs) that emit tunable, strong, and stable fluorescence. The synthesis of BPLPs and CBPLPs was straightforward and cost-effective. BPLP families possess excellent processability for micro/nano fabrication and desired mechanical properties, potentially serving as implant materials and bioimaging probes *in vitro* and *in vivo*. Preliminary data show that CBPLPs support cell attachment *in vitro* and only exert weak chronic inflammation *in vivo*. The development of BPLPs and CBPLPs represent a new direction in developing biodegradable materials and may have wide impact on basic sciences and a broad range of applications such as tissue engineering, drug delivery, and bioimaging.

Methods

Synthesis and Characterization of BPLPs and CBPLPs. For BPLP synthesis, equimolar amounts of citric acid and 1,8-octanediol were combined and stirred with additional L-cysteine at molar ratios of L-cysteine/citric acid 0.2, 0.4, 0.6, and 0.8. After melting the mixture at 160 °C for 20 min, the temperature was brought down to 140 °C stirring continuously for another 75 min to obtain the BPLP-cysteine (BPLP-Cys) oligomers or low-molecular-weight compounds. The oligomers were purified by precipitating the oligomer/1,4-dioxane solution in water followed by freeze drying. Each of the 20 (L-) amino acids was used to synthesize a family of BPLP-amino acid polymers. Water soluble polymer (BPLP-PEG-amino acid) was synthesized using poly PEG, citric acid, and amino acid. Other aliphatic diols (C₃–C₁₂ diols) can also be used for BPLP synthesis similar to our previously developed poly(diols citrates) (24). The synthesized BPLPs have a shelf-life of over a year without significant changes on their photoluminescent properties (emission wavelength and intensity) when stored in amber glass bottles at –20 °C (Fig. S6).

For CBPLP film synthesis, BPLP was dissolved in 1,4-dioxane to form a 30 wt. % solution and then cast into a Teflon mold followed by solvent evaporation and then postpolymerization at 80 °C for 4 days. For CBPLP scaffold fabrication, a common salt-leaching method was applied (36). For BPLP nanoparticle preparation, 0.6 g of BPLP was dissolved in acetone (10 mL). The polymeric solution was added dropwise to deionized water (30 mL) under magnetic stirring (400 rpm). The setup was left overnight in a chemical hood to evaporate the acetone. TEM (JEOL-1200 EX II) and dynamic light scattering (DLS, Microtrack) were used to determine the size, shape, and size distribution of the nanoparticles. The BPLPs were characterized by Fourier Transform Infrared (FT-IR), ¹H- and ¹³C-NMR (NMR), and matrix-assisted laser desorption/ionization mass spectroscopy (MALDI-MS; Bruker Autoflex).

Photoluminescent Properties. Photoluminescence spectra of BPLP-Cys-0.2 solutions and nanoparticles, and CBPLP-Cys-0.2 films and scaffolds were acquired on a Shimadzu RF-5301 PC fluorospectrophotometer. Both the excitation and the emission slit widths were set at 1.5 nm for all samples unless otherwise stated. The Williams method was used to measure the fluorescent quantum yield of the BPLP polymers (37). The photostability of BPLP-Cys solution, BPLP-Cys film, BPLP-Ser solution, and Rhodamine B solution were evaluated by recording the changes of the fluorescence intensity of the samples under continuous excitation in the fluorospectrophotometer. The excitation wavelength for photostability tests was deter-

mined by the maximum absorbance spectra of each type of sample. The fluorescence changes with degradation were determined by measuring the fluorescence intensity of the solutions of BPLP-Cys degraded in 0.05 M NaOH under 37 °C at various degradation degrees and at the same concentration.

Mechanical Tests and Degradation Studies. The tensile mechanical tests on CBPLP films were conducted according to ASTM D412a on a MTS Insight 2 mechanical tester (24). The initial modulus was measured from a slope of stress-strain curve at 10% of strain. The compressive tests on CBPLP scaffold (90% porosity, 100 μm pore size, 3 mm height, 6 mm diameter) were conducted according to a method described in ref. 30. The *in vitro* degradation of BPLP and CBPLP polymers were conducted by incubating the polymers in PBS (pH = 7.4) at 37 °C for various times to obtain polymer mass loss (36). To analyze the degradation products of the BPLPs, 3 grams of BPLPs were degraded in 0.05 M NaOH for 24 h and in 1 M NaOH for 48 h. Soluble degradation products were investigated by high performance liquid chromatography – electrospray ionization – mass spectrometry (HPLC-ESI-MS; Shimadzu LCMS-2010), using hydrophilic interaction chromatography (HILIC) on an amide-bonded stationary phase (Tosoh Bioscience Amide-80). The filtered (0.2 μm PTFE syringe filter; Whatman), *in vitro* degraded sample of BPLP-Cys was analyzed to track the presence of monomers based on retention time and mass-to-charge ratio (matched to the analysis of standards) in the negative ionization mode.

Cytotoxicity Evaluation. Mouse 3T3 fibroblasts were used to evaluate the cytocompatibility of the polymers. The cell viability and proliferation on CBPLP-Cys-0.2 and CBPLP-Ser-0.2 films (80 °C for 4 days) was determined by methylthiazolotetrazolium (MTT) assay as described in ref. 36. The cell morphology was observed under scanning electron microscopy (SEM, Hitachi 3500N). Cytotoxicity of the polymer degradation products was investigated according to a method described elsewhere (38). Briefly, BPLP-Cys, BPLP-Ser and their CBPLPs (80 °C for 4 days) were hydrolytically degraded in 1M NaOH solution at 37 °C over a period of 24 h to 72 h. The solution was then filtered through a cellulose acetate membrane syringe filter (0.2 μm pore diameter). The pH was adjusted to 7.4 with 1 M HCl. The solution was filtered again for sterilization and then diluted by 2, 10, 50, and 100 times with culture medium. The solutions were added to the cultured cells (*n* = 5 wells for each polymer dilution) in 96-well plates (100 μL per well) and incubated at 37 °C and 5% CO₂ for 24 h. Cell viability was then determined using MTT assay. POC (80 °C, 4 d) and poly(D,L-lactide-co-glycolide) (PLGA75/25, Mw = 113 kDa; Lakeshore Biomaterials) were used as controls for the above cytotoxicity evaluation. The statistical significance between 2 sets of data were calculated using a Student's *t* test. Data were considered to be significant when *P* ≤ 0.05 was obtained (showing a 95% confidence limit).

Bioimaging Studies *In Vitro* and *In Vivo*. For cellular fluorescence-labeling *in vitro*, 3T3 mouse fibroblasts were seeded on sterile glass cover slips at a density of 5,000 cells per mL for 24 h before the cellular uptake study. The cover slips were washed with PBS and transferred to new Petri dishes, and then incubated with a BPLP-Ser-0.2 nanoparticle solution in PBS (2% wt, 80 nm in diameter) for 4 h at 37 °C. At the end of the study, the cells were washed (PBS × 3) and then fixed with glutaraldehyde solution (2.5%). Cells were observed under a Leica DMLP microscope (Nikon). For nanoparticle/scaffold bioimaging *in vivo*, BPLP-Ser-0.2 nanoparticles [2% wt in PBS, 80 nm in diameter, sterilized by filtering through a syringe filter (0.22 μm)] and CBPLP-Ser-0.2 scaffolds (6 mm in diameter, 90% porosity, 100 μm pore size, 1.5 mm thick, sterilized by 70% ethanol and UV light) were injected/implanted *s.c.* in nude mice (BALB/c nu/nu). The mice were then imaged using a CRi Maestro Imaging System, as described previously (14, 39), immediately after the implantation. CBPLP-Ser scaffolds *s.c.* implanted in nude mice for 5 months (*n* = 4) were sectioned for hematoxylin and eosin (H&E) staining to preliminarily evaluate the long-term *in vivo* host responses to the polymers. Animals were cared for in compliance with the regulations of the animal care and use committee of The University of Texas Southwestern Medical Center.

For further details, see *SI Methods*.

ACKNOWLEDGMENTS. This work was supported in part by an American Heart Association Beginning Grant-in-Aid award (to J.Y.), the UTA Research Enhancement Program (J.Y.), National Institutes of Health grants (to L.T), and the Shimadzu Equipment Grants for Research program (K.A.S.). The CRi Maestro was purchased with funds from the U.S. Department of Energy Grant DE-FG02-05CH11280), and *in vivo* imaging was facilitated by the SW-SAIR, which is supported by an National Cancer Institute U24 CA126608 and the Simmons Cancer Center.

1. Brus L (1991) Quantum crystallites and nonlinear optics. *Appl Phys A* 53:465–474.
2. Nirmal M, Brus L (1999) Luminescence photophysics in semiconductor nanocrystals. *Acc Chem Res* 32:407–414.
3. Klimov VL, et al. (2000) Optical gain and stimulated emission in nanocrystal quantum dots. *Science* 290:314–317.
4. Coe S, Woo WK, Bawendi MG (2002) Electroluminescence from single monolayers of nanocrystals in molecular organic devices. *Nature* 420:800–803.
5. Wozniak AK, et al. (2008) Single-molecule FRET measures bends and kinks in DNA. *Proc Natl Acad USA* 105:18337–18342.
6. Wang H, et al. (2005) In vitro and in vivo two-photon luminescence imaging of single gold nanorods. *Proc Natl Acad USA* 102:15752–15756.
7. Waggoner A (2006) Fluorescent labels for proteomics and genomics. *Curr Opin Chem Biol* 10:62–66.
8. Lopez-Crapez E, et al. (2008) A homogeneous resonance energy transfer-based assay to monitor MutS/DNA interactions. *Anal Biochem* 383:301–306.
9. Thurn KT, et al. (2007) Nanoparticles for applications in cellular imaging. *Nanoscale Res Lett* 2:430–441.
10. Wang F, et al. (2006) Luminescent nanomaterials for biological labelling. *Nanotechnology* 17:R1–R13.
11. Gao X, et al. (2005) In vivo molecular and cellular imaging with quantum dots. *Curr Opin Biotech* 16:63–72.
12. Jamieson T, et al. (2007) Biological applications of quantum dots. *Biomaterials* 28:4717–4732.
13. Michalet X, et al. (2005) Quantum dots for live cells, in vivo imaging, and diagnostics. *Science* 307:538–544.
14. Su J, et al. (2008) Exploring feasibility of multicolored CdTe quantum dots for in vitro and in vivo fluorescent imaging. *J Nanosci Nanotechnol* 8:1174–1177.
15. Mauring K, Krasnenko V, Miller S (2007) Photophysics of the blue fluorescent protein. *J Lumin* 122:291–293.
16. Yanushevich YG, et al. (2002) A strategy for the generation of non-aggregating mutants of Anthozoa fluorescent proteins. *FEBS L* 511:11–14.
17. Nie SM, Xing Y, Kim GJ, Simons JW (2007) Nanotechnology applications in cancer. *Annu Rev Biomed Eng* 9:257–288.
18. Mancini MC, Kairdolf BA, Smith AM, Nie S (2008) Oxidative quenching and degradation of polymer-encapsulated quantum dots: New insights into the long-term fate and toxicity of nanocrystals in vivo. *J Am Chem Soc* 130:10836.
19. Huang SP, Huang GS, Chen SA (2007) Deep blue electroluminescent phenylene-based polymers. *Synth Met* 157:863–871.
20. Gaumet M, Gurny R, Delie F (2007) Fluorescent biodegradable PLGA particles with narrow size distributions: Preparation by means of selective centrifugation. *Int J Pharm* 342:222–230.
21. Ogura Y, Kimura H (1995) Biodegradable polymer microspheres for targeted drug-delivery to the retinal-pigment epithelium. *Surv Ophthalmol* 39:S17–S24.
22. Ghoroghchian PP, et al. (2007) Controlling bulk optical properties of emissive polymeric microspheres through intramembranous polymer-fluorophore interactions. *Chem Mater* 19:1309–1318.
23. Rhyner MN, et al. (2006) Quantum dots and multifunctional nanoparticles: New contrast agents for tumor imaging. *Nanomedicine* 1:209–217.
24. Yang J, et al. (2006) Synthesis and evaluation of poly(diols citrate) biodegradable elastomers. *Biomaterials* 27:1889–1898.
25. Yang J, Webb AR, Ameer GA (2004) Novel citric acid-based biodegradable elastomers for tissue engineering. *Adv Mater* 16:511–516.
26. Mulliken RS (1939) Intensities of electronic transitions in molecular spectra IV. Cyclic dienes and hyperconjugation. *J Chem Phys* 7:339–352.
27. Bruggeman JP, et al. (2008) Biodegradable xylitol-based polymers. *Adv Mater* 20:1922–1927.
28. Wang Y, Ameer GA, Sheppard BJ, Langer R (2002) A tough biodegradable elastomer. *Nat Biotechnol* 20:602–606.
29. Yang J, et al. (2006) Modulating expanded polytetrafluoroethylene vascular graft host response via citric acid-based biodegradable elastomers. *Advanced Materials* 18:1493–1498.
30. Yang J, Motlagh D, Webb AR, Ameer GA (2005) Novel biphasic elastomeric scaffold for small-diameter blood vessel tissue engineering. *Tissue Eng* 11:1876–1886.
31. Yang J, et al. (2008) Fluorescent magnetic nanohybrids as multimodal imaging agents for human epithelial cancer detection. *Biomaterials* 29:2548–2555.
32. Altschuh D, Oncul S, Demchenko AP (2006) Fluorescence sensing of intermolecular interactions and development of direct molecular biosensors. *J Mol Recognit* 19:459–477.
33. Langer R, Vacanti JP (1993) Tissue engineering. *Science* 260:920–926.
34. Levenberg S, Langer R (2004) Advances in tissue engineering. *Curr Top Dev Biol* 61:113–134.
35. Nijst CL, et al. (2007) Synthesis and characterization of photocurable elastomers from poly(glycerol-co-sebacate). *Biomacromolecules* 8:3067–3073.
36. Yang J, et al. (2002) Fabrication and surface modification of macroporous poly(L-lactic acid) and poly(L-lactic-co-glycolic acid) (70/30) cell scaffolds for human skin fibroblast cell culture. *J Biomed Mater Res* 62:438–446.
37. Williams ATR, Winfield SA, Miller JN (1983) Relative fluorescence quantum yields using a computer-controlled luminescence spectrometer. *Analyst* 108:1067–1071.
38. Timmer M, et al. (2003) In vitro cytotoxicity of injectable and biodegradable poly(propylene fumarate)-based networks: Unreacted macromers, cross-linked networks, and degradation products. *Biomacromolecules* 4:1026–1033.
39. Zhang J, et al. (2008) Evaluation of red CdTe and near infrared CdHgTe quantum dots by fluorescent imaging. *J Nanosci Nanotechnol* 8:1155–1159.